Optik - International Journal for Light and Electron Optics 207 (2020) 164448

Contents lists available at ScienceDirect

Optik

journal homepage: www.elsevier.com/locate/ijleo

Original research article

Spatial confinement effect on CN emission from nanosecond laser-induced PMMA plasma in air

Junfeng Shao[a], Jin Guo[a], Qiuyun Wang[b,c], Anmin Chen[b,c,*], Mingxing Jin[b,c,*]

[a] State Key Laboratory of Laser Interaction With Matter & Innovation Laboratory of Electro-Optical Countermeasures Technology, Changchun Institute of Optics, Fine Mechanics and Physics, Chinese Academy of Sciences, Changchun, 130033, China
[b] Institute of Atomic and Molecular Physics, Jilin University, Changchun, 130012, China
[c] Jilin Provincial Key Laboratory of Applied Atomic and Molecular Spectroscopy (Jilin University), Changchun, 130012, China

ARTICLE INFO

Keywords:
Laser-induced breakdown spectroscopy
Spatial confinement
CN
PMMA

ABSTRACT

In this paper, a PMMA target was ablated to study spatial confinement effect on CN emission of laser-induced breakdown spectroscopy in air. Four cylindrical cavities with same depth and different diameters (4, 6, 8, and 10 mm) were used to confine the nanosecond laser-ablated PMMA plasma plume. Laser pulse energies were 40, 50, and 60 mJ. The influence of cavity diameter on emission band and vibration temperature of CN molecule was demonstrated, the results showed an obvious increase in the emission and vibration temperature of CN molecule by using the cylindrical cavity. When the cavity diameter was smaller at a fixed laser energy, the emission enhancement of CN molecule appeared earlier, and the CN molecule had stronger emission and vibration temperature. For a fixed diameter cavity, when the laser energy was higher, the CN molecule presented stronger emission and higher vibration temperature, and the emission enhancement also appeared earlier. The enhanced effect on the spatial confinement mainly comes from shock wave produced by the laser-induced PMMA plasma. The spatial confinement cavity can reflect the shock wave, and the shock wave compresses the plasma plume, resulting in an improvement in the temperature and density of the plasma. Therefore, the optical emission of CN molecule increases as the shock wave interacts with the PMMA plasma.

1. Introduction

Laser-induced breakdown spectroscopy (LIBS) is a type of atomic emission spectroscopy (AES) [1]. Due to LIBS advantages of simple operation, low cost, and wide detection range (solid, liquid, and gas) [2–7], LIBS has become most practical, widely used and popular element analysis technology. Its basic principle is to focus high-energy pulsed laser on sample surface to be measured, producing brightness plasma with extremely high temperature and density. In the processes of the plasma cooling, atoms and ions in the plasma will transition to a lower energy level or ground state from high excited state. During the transition, specific photons are emitted to generate characteristic spectral lines, and frequency and intensity of the spectral lines contain the species and concentration information on the composition elements of the sample. At present, molecular emission is also a hot topic in LIBS. The molecular emission from LIBS plays a significant role in the application of composition analysis [8–10], can present more chemical information for the detection of organic compounds [11,12]. Dietz et al. reported an improved analysis of chlorides in cement and concrete using molecular LIBS [13]. Harilal et al. provided an review on optical spectroscopy of laser-induced plasmas for standoff

* Corresponding authors at: Institute of Atomic and Molecular Physics, Jilin University, Changchun, 130012, China.
E-mail addresses: amchen@jlu.edu.cn (A. Chen), mxjin@jlu.edu.cn (M. Jin).

https://doi.org/10.1016/j.ijleo.2020.164448
Received 13 January 2020; Accepted 17 February 2020

isotopic analysis [14]. Rao et al. discussed the correlation between molecular structure and LIBS data for femtosecond and nanosecond LIBS of nitroimidazoles [15]. Wang et al. investigated the influence of the distance from sample surface to geometric focus on the emission intensity of CN molecule in femtosecond LIBS of PMMA [16].

Although LIBS technology has many unique advantages, its high detection limit compared with inductively coupled plasma mass spectrometry results in poor detection sensitivity, making it difficult to perform qualitative and quantitative analysis on low-concentration elements. Therefore, researchers have developed many methods to improve the characteristic line intensity, such as double-pulse configuration [17–23], magnetically confined LIBS [24–26], spark-discharge-assisted LIBS [27–29], preheated-sample LIBS [30–33], and introducing inert gas [34–38]. However, the methods above all have their own disadvantages, such as double-pulse LIBS: on the one hand, it increases the complexity of LIBS installation; on the other hand, the use of more than one laser increases the cost. For magnetically confined LIBS, due to the instability of the magnetic field, the confinement effect is not very stable, and there are too many uncertain factors. The introduction of inert gas has more complicated operation. After comparison, it is found that a simple, flexible and low-cost method is spatially confined LIBS. The spatially confined LIBS is mainly based on shock wave produced by laser-induced plasma. The shock wave propagates at supersonic velocity, that is, the shock wave travels much faster than the plasma. Adding a spatial confinement device can confine the shock wave, so that the diffused shock wave is reflected back through the interface to confine and compress the plasma [39–41]. Many researchers have carried out specific studies on spatially confined LIBS. Shen et al. focused a beam of laser to ablate aluminum target to generate plasma in air, using a pair of parallel plates to confine the plasma, and the plasma emission was increased up to 6 times when the distance between two plates was 10 mm and delay time was 11 μs [42]. Li et al. ablated copper target to generate laser-induced plasma in air, cylindrical cavities with different depths and diameters were used to confine the plasma, the emission intensity of copper atomic lines was improved after several microseconds [43]. Wang et al. discussed the role of cavity shape on spatially confined LIBS, the cavity with different shapes and same depth was used to confine the plasma, the emission intensity and plasma temperature were significantly improved [40].

For spatial confinement mentioned above, many papers have investigated the characteristics of atomic and ionic spectra under spatial confinement, while very few studies have focused on the characteristics of molecular spectra under spatial confinement. In this paper, we used a Q-switched Nd:YAG laser to ablate PMMA sample and investigate the influence of spatial confinement on spectral emission of CN molecule. Four cylindrical cavities (4, 6, 8, and 10 mm) with 6 mm depth were used to confine the laser-induced PMMA plasmas. We measured time-resolved optical emission of CN molecule in PMMA plasma and obtained corresponding vibration temperature.

2. Experimental setup

The experimental setup for spatially confined laser-induced PMMA plasma spectroscopy is presented in Fig. 1. The entire experimental process was in air environment. Four cylindrical confinement cavities with 6 mm depth were used to confine the PMMA plasma, with diameters of 4, 6, 8 and 10 mm, respectively. The excitation light source was a Q-switched Nd: YAG laser (Continuum, Surelite III), and its wavelength, pulse width, and repetition frequency were 1064 nm, 10 ns, and 10 Hz, respectively. The laser energies used in the experiment were 40, 50 and 60 mJ, respectively. We used each laser pulse to trigger a photodiode to synchronize the delay between laser pulse and spectral signal, and set the photodiode signal to time zero. The laser pulse passed through an iris (I), and was reflected by a mirror (M). The reflected laser pulse was focused by a plano-convex quartz lens (L) with a focal length of 10 mm, and then irradiated perpendicularly on the surface of the PMMA target through the centre of the cylindrical cavity. The cylindrical confinement cavity was tightly close to the surface of the PMMA target. The PMMA target was placed on a precision three-dimensional translation stage (Thorlabs, PT3/M-Z8) controlled by a computer. After the laser ablation of the PMMA sample, the plasma was ejected from the surface of the sample, and was located in the center of the cylindrical confinement cavity. The plasma emission was focused into a fiber through the focusing lens, a dichroic mirror (DM), and another lens (BK7, 75 mm focal length). The fiber was fixed on another three-dimensional translation stage to align the light collection. The other end of the fiber was connected

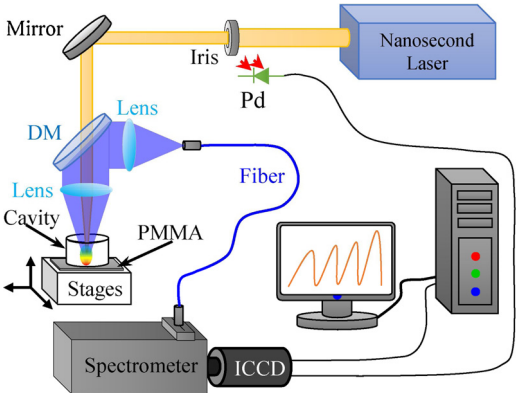

Fig. 1. Experimental setup for laser-induced PMMA plasma spectroscopy under spatial confinement (Pd, photodiode; DM, dichroic mirror; L, lens; I, iris; and ICCD, intensified CCD; M, mirror).

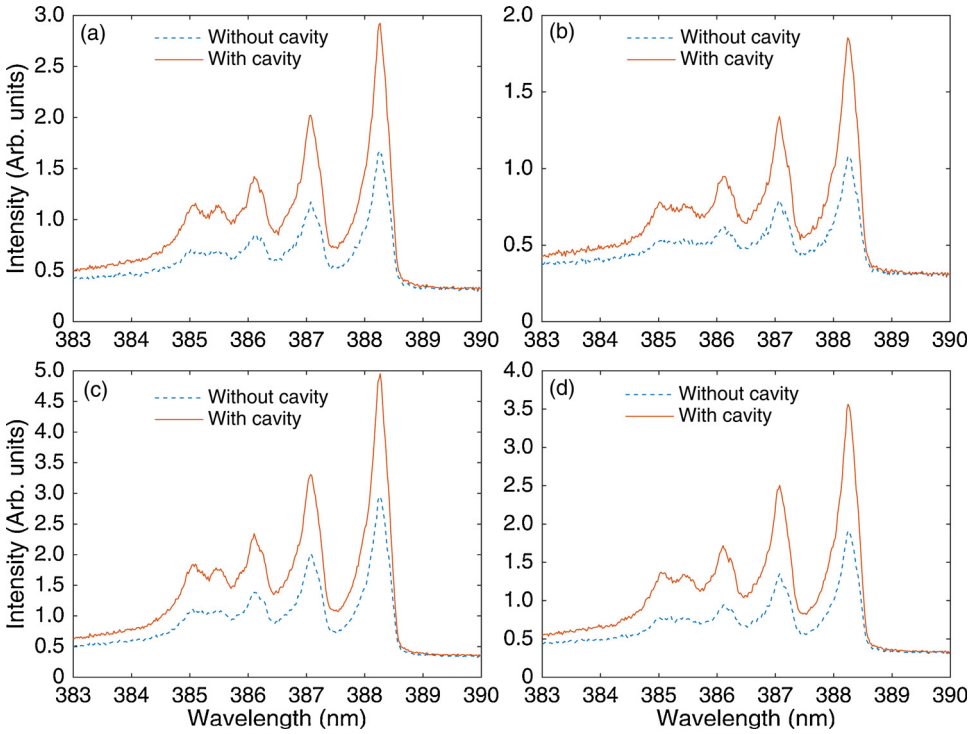

Fig. 2. Spectral bands of CN molecules with (solid line) and without (dashed line) spatial confinement. (a) Laser energy is 50 mJ; delay time is 3.5 μs; cavity diameter is 6 mm. (b) Laser energy is 50 mJ; delay time is 5.0 μs; cavity diameter is 8 mm. (c) Laser energy is 60 mJ; delay time is 3.0 μs; cavity diameter is 6 mm. (d) Laser energy is 60 mJ; delay time is 4.5 μs; cavity diameter is 8 mm.

to a spectrometer (Princeton Instruments, PI Acton, Spectra Pro 500i) with an ICCD detector (Princeton Instruments, PI Acton, Spectra Pro 500i) for detecting spectral signal. The grating used in the spectrometer was 1200 lines / mm. The ICCD camera worked at a gated mode, and the corresponding gate width was 0.5 μs. In order to enhance the spectral stability and reduce the measured error, each spectrum was the accumulation of 50 laser shots.

3. Results and discussion

Fig. 2 shows spectral bands of CN molecules in a wavelength range of 383 ~ 390 nm with (solid lines) and without (dashed lines) spatial confinement. Five emission spectral peaks can be clearly observed, which are distributed in the CN molecule band emission of the violet system ($B^2\Sigma^+ - X^2\Sigma^+$) of the sequence $\Delta\nu = 0$. The five CN peaks are 388.29 nm, 387.0 nm, 386.14 nm, 385.44 nm, and 385.03 nm with the vibration transitions of (0-0), (1-1), (2-2), (3-3) and (4-4), respectively, and the (0-0) transition line is the strongest emission peaks [11,12]. From Fig. 2, we can know three pieces of information. First, the intensity of spectral band of the CN molecule with the cylindrical confinement cavity is much stronger than that without the cylindrical cavity. Second, at the same laser energy (50 or 60 mJ), the intensity of the CN molecular band with a smaller cavity diameter (6 mm) is stronger than that with a larger cavity diameter (8 mm), comparing Fig. 2(a) and (b) or Fig. 2(c) and (d). The shock wave compression effect decreases with increasing the diameter of confinement cavity, that is, the smaller the diameter, the better the compression effect of the shock wave. Third, at the same cavity diameter (6 or 8 mm), the intensity of the CN molecular band with high energy (60 mJ) is stronger than that with low energy (50 mJ), comparing Fig. 2(a) and (c) or Fig. 2(b) and (d). When the laser energy is small, the shock wave generated by the laser-induced plasma is slow and the pressure is relatively small [44]. Therefore, the spatial confinement of the plasma is weak, and the enhancement of spectral emission is low. However, high laser energy is used to produce laser-induced plasma, the plasma plume is bigger accompanied by stronger shock wave, and the spectral emission is also stronger [45,46]. To investigate the effect of cavity diameter and laser energy on the emission intensity of CN molecule in LIBS, the time-resolved spectra of the PMMA plasmas were obtained.

Laser ablation mainly goes through three stages: (1) laser irradiation of sample leads to material evaporation; (2) the interaction between evaporated material and laser forms laser-induced plasma; (3) the plasma expands and cools rapidly. The most interesting part in three stages is dynamic evolution of the plasma plume [45,47]. LIBS is a dynamic decay process, and time-resolved spectra are important for studying the various characteristics of the plasma. The time-resolved emission spectra of the CN molecular band at the sequence $\Delta\nu = 0$ were measured. The (0-0) transition of the CN molecular band was used to understand the dynamic decay process of LIBS because it has strongest emission intensity compared to other peaks. Fig. 3 presents the time-resolved peak emission of CN (0-0) with and without the cylindrical cavities for 50 and 60 mJ laser energies. Lines marked with different shapes represent different

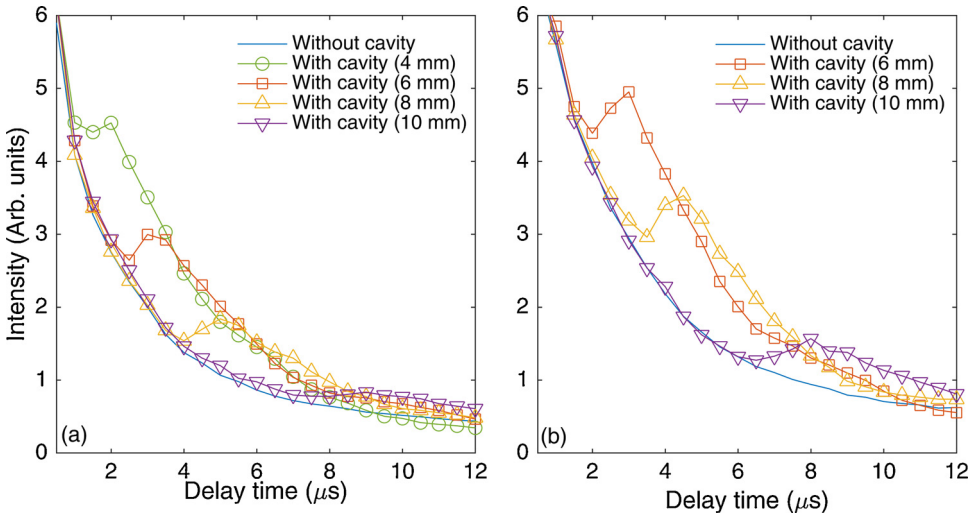

Fig. 3. Time-resolved peak emission of CN (0-0) with and without the cylindrical cavities for 50 and 60 mJ laser energies.

diameters. From Fig. 3(a), without spatial confinement, the CN (0-0) emission intensity continuously drops with increasing the delay time. When the delay time is longer than 10 μs, the CN (0-0) emission intensity remains unchanged basically. In the case with cylindrical confinement cavities, the CN (0-0) emission firstly decays in earlier delay stage. When the delay time reaches a certain value, the CN (0-0) emission increases, and then begins to decay after reaching a maximum value. This is because the laser pulse ablated the PMMA target to generate the plasma accompanied by the generation of the shock wave, and the diffusion speed of the shock wave is much faster than that of the plasma plume. The faster expanding shock wave is reflected by the inner wall of the cylindrical cavity, and the reflected shock wave interacts with the expanding plume, resulting in the enhancement of the CN (0-0) emission from the plasma [48–51]. The trend in the CN (0-0) emission with delay time at 60 mJ laser energy is similar to that at 50 mJ laser energy.

Taking 4 mm cylindrical cavity with 50 mJ laser energy (see Fig. 3(a)) as an example, the CN (0-0) emission decreases in earlier delay time. At approximately 1.0 μs delay time, the CN (0-0) emission begins to increase, indicating that the shock wave took 1.0 μs from generation to being reflected to interaction with the plasma. Then the duration of the interaction with the plasma is also approximately 1.0 μs, and the enhancement effect of the molecular band reaches a maximum. After that, the shock wave no longer interacts with the plasma, the plasma continues to expand and cool, and the intensity of the CN (0-0) emission begins to decrease gradually. The time-resolved peak emission of the CN (0-0) with different diameter cavities at same laser energy reveals that: first, as the diameter of the confinement cavity increases, the delay time for the enhancement of the CN (0-0) emission becomes longer, that is, the traveling distance and time of the shock wave will increase with the increase in the cavity diameter; second, as the diameter of the confinement cavity increases, the enhancement effect of the CN (0-0) emission becomes weaker. During the traveling of the shock wave, it will consume a lot of energy. The bigger the cavity diameter, the longer the traveling distance; and the shock wave will consume more energy. By comparing the sequences in Fig. 3(a) and (b), it is found that the higher laser excitation energy, the stronger emission. This reveals that laser energy plays a significant role in the CN (0-0) peak intensity. Comparing the cases with same diameter cavities (6, 8, and 10 mm) for different laser energies (see Fig. 3(a) and (b)), the corresponding enhancement is more obvious at high laser energy (60 mJ). For example, as the diameter of the cavity is 10 mm, a significant enhancement in the range of delay time from 6 μs to 12 μs can be observed at 60 mJ laser energy, while the enhancement in the range of delay time from 8 μs to 12 μs is not obvious in the case of 50 mJ. This is because higher laser energy ablates the sample to generate stronger shock wave [45]. The stronger shock wave compresses the plasma plume, resulting in more obvious enhancement effect. Through the discussion mentioned above, both the cavity diameter and the laser energy have an influence on the delay time for maximum emission enhancement of CN (0-0).

Fig. 4 shows the histogram of the delay time for maximum enhancement at different diameters (4, 6, 8, and 10 mm) and energies (40, 50, and 60 mJ). From the figure, it can be clearly observed that both the laser energy and the cavity diameter affect the delay time for maximum enhancement. Taking 50 mJ laser energy as an example, when the cavity diameters are 4, 6, 8 and 10 mm, the corresponding maximum enhanced delay times are about 2.0, 3.5, 5.0, and 9.0 μs, respectively. As the cavity diameter increases, the traveling distance of the shock wave increases. The traveling time of the shock wave becomes longer, resulting in an increase in the delay time of the interaction between the shock wave and the plasma. Taking 8 mm cavity diameter as an example, when the laser energy is 40, 50 and 60 mJ, the corresponding maximum enhanced delay time are about 7.0, 5.0, and 4.5 μs, respectively. For higher laser energy, stronger shock wave can be generated compared with lower laser energy. The stronger shock wave is faster and the traveling time is shorter, resulting in a shorter delay time for maximum emission enhancement.

The vibration temperature of molecular spectral band is useful parameter for describing various properties of molecular emission, and can help us better understand the various dynamic process of molecular emission. To do this, we need to calculate the physical parameter. Fig. 5 presents the comparison of measured and fitted spectral bands of CN molecules ($\Delta\nu = 0$). By observing the

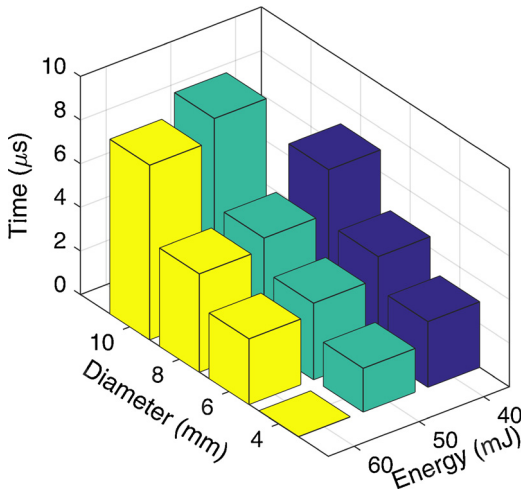

Fig. 4. Histogram of delay time for maximum enhancement at different diameters (4, 6, 8, and 10 mm) and energies (40, 50, and 60 mJ).

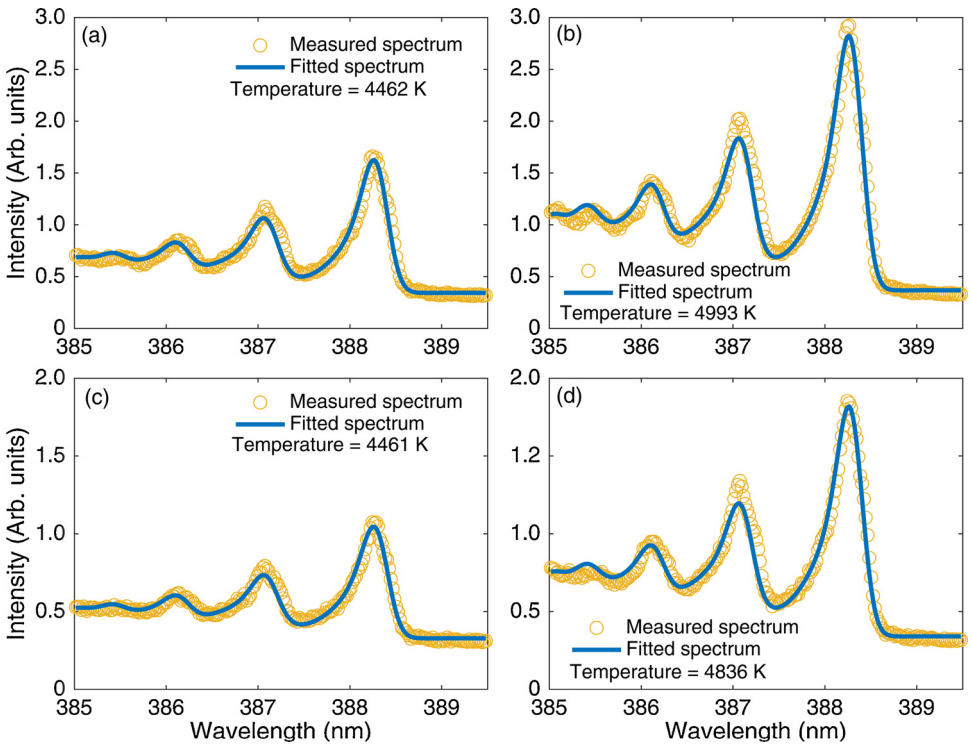

Fig. 5. Comparison of measured and fitted spectral bands of CN molecules ($\Delta\nu = 0$). Laser energy is 50 mJ. (a) CN band without cavity, delay time is 3.5 μs. (b) CN band with 6 mm diameter cavity, delay time is 3.5 μs. (c) CN band without cavity, delay time is 5.0 μs. (d) CN band with 8 mm diameter cavity, delay time is 5.0 μs.

measured spectral band, the CN molecular spectrum measured in the experiment can fit the theoretical model better [12,14,52–55]. The fitting results show that the vibration temperatures are 4462 K (a), 4993 K (b), 4461 K (c), and 4836 K (d) in Fig. 5. The vibration temperature of CN molecule in LIBS can be obtained.

Fig. 6 shows the evolution of vibration temperature of CN molecule ($\Delta\nu = 0$) with the delay time for 50 and 60 mJ laser energies. The trend in the vibration temperature of CN molecule ($\Delta\nu = 0$) with the change in the delay time is similar to that in the emission peak of CN (0-0) (see Fig. 3). In the case without cylindrical cavity, the vibration temperature of CN molecule decreases monotonously with the increase of the delay time. As a cylindrical confinement cavity is introduced, the vibration temperature of CN molecule ($\Delta\nu = 0$) will increase first and then decrease with increasing the delay time. The reflected shock wave by the inner wall of the cylindrical cavity compresses the plasma plume to a smaller volume, leading to an increase in the collision rate with the plasma plume. Therefore, the vibration temperature of CN molecule ($\Delta\nu = 0$) increases in a period of the delay time. For 50 mJ laser energy,

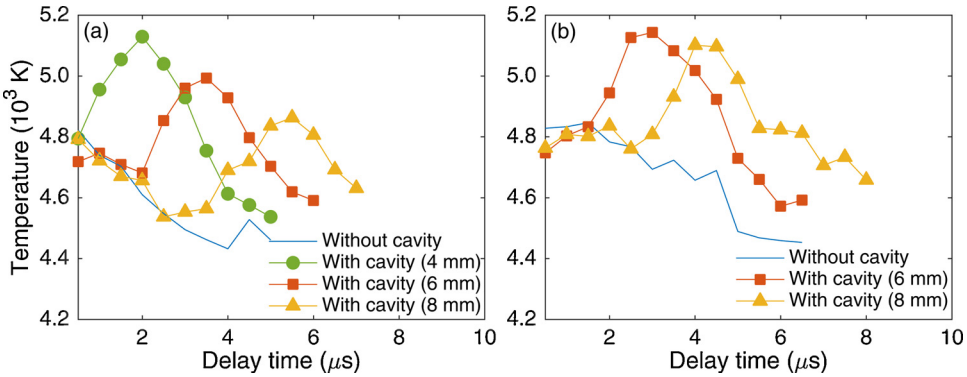

Fig. 6. Evolution of vibration temperatures of CN molecules with the delay time for 50 and 60 mJ laser energies.

as the cavity diameters are 4, 6, and 8 mm, the maximum vibration temperatures of CN molecule ($\Delta\nu = 0$) are about 5140, 4990, and 4850 K, respectively. The diameter of the cavity is inversely proportional to the pressure of the shock wave. The bigger the cavity diameter, the weaker the compression effect of shock wave on plasma plume, the lower the collision rate between particles, and the lower the vibration temperature of CN molecule ($\Delta\nu = 0$). At same diameter (e.g. 6 mm), comparing two laser energies (50 and 60 mJ), the corresponding maximum vibration temperatures of CN molecules ($\Delta\nu = 0$) are about 4990 and 5160 K, respectively. This is because the higher laser energy generates the stronger shock wave, the stronger shock wave can compress plasma more effectively, resulting in the higher vibration temperature of CN molecule. In summary, both the cavity diameter and the laser energy can affect the vibration temperature of CN molecule.

4. Conclusions

To investigate the emission enhancement effect of spatial confinement on CN molecular band ($\Delta\nu = 0$) of laser-induced PMMA plasma, the cylindrical cavities with different diameters (4, 6, 8, and 10 mm) were used to confine the plume of the laser-ablated PMMA plasma. The time-resolved spectral band intensity and vibration temperature of CN molecule with and without cylindrical cavities for different laser energies were compared and analyzed. The results showed that the enhancement in the CN molecular band and vibration temperature is related to the cavity diameter and laser energy. The bigger the cavity diameter, the longer the delay times for maximum enhancement; the enhanced effect of the CN molecular band became weaker as the diameter of the cavity increases; at higher laser energy, the spectral enhancement appeared earlier, and is also more obvious. The spatial confinement by using the cylindrical cavity can improve the signal sensitivity of molecular spectra in LIBS.

Declaration of Competing Interest

The authors declare that there are no conflicts of interest.

Acknowledgments

We acknowledge the support by the National Natural Science Foundation of China (Grant Nos. 11674128, 11674124, and 11974138); the Jilin Province Scientific and Technological Development Program, China (Grant No. 20170101063JC).

References

[1] J.D. Winefordner, I.B. Gornushkin, T. Correll, E. Gibb, B.W. Smith, N. Omenetto, Comparing several atomic spectrometric methods to the super stars: special emphasis on laser induced breakdown spectrometry, LIBS, a future super star, J. Anal. Atom. Spectrom. 19 (2004) 1061–1083.
[2] M. Tran, Q. Sun, B.W. Smith, J.D. Winefordner, Determination of F, Cl, and Br in solid organic compounds by laser-induced plasma spectroscopy, Appl. Spectrosc. 55 (2001) 739–744.
[3] P. Fichet, P. Mauchien, J.F. Wagner, C. Moulin, Quantitative elemental determination in water and oil by laser induced breakdown spectroscopy, Anal. Chim. Acta 429 (2001) 269–278.
[4] J. Gruber, J. Heitz, H. Strasser, D. Bauerle, N. Ramaseder, Rapid in-situ analysis of liquid steel by laser-induced breakdown spectroscopy, Spectrochim. Acta Part B At. Spectrosc. 56 (2001) 685–693.
[5] D. Zhang, A. Chen, Q. Wang, W. Xu, Y. Wang, S. Li, Y. Jiang, M. Jin, Influence of distance between sample surface and focal point on the expansion dynamics of laser-induced silicon plasma under different sample temperatures in air, Optik 202 (2020) 163511.
[6] Y. Li, H.Z. Zhang, Z.K. Jiang, Z.S. Li, C.H. Hu, Spectroscopic characterization of aluminum plasma using laser-induced breakdown spectroscopy, Optik 125 (2014) 2851–2855.
[7] A.M. Chen, Y.F. Jiang, H. Liu, M.X. Jin, D.J. Ding, Plume splitting and rebounding in a high-intensity CO2 laser induced air plasma, Phys. Plasmas 19 (2012) 073302.
[8] S. Carter, A. Fisher, R. Garcia, B. Gibson, J. Marshall, I. Whiteside, Atomic spectrometry update: review of advances in the analysis of metals, chemicals and functional materials, J. Anal. Atom Spectrom 31 (2016) 2114–2164.
[9] S. Rai, A.K. Rai, Characterization of organic materials by LIBS for exploration of correlation between molecular and elemental LIBS signals, AIP Adv. 1 (2011) 042103.
[10] Q. Wang, A. Chen, W. Xu, D. Zhang, Y. Wang, S. Li, Y. Jiang, M. Jin, Effect of lens focusing distance on AlO molecular emission from femtosecond laser-induced aluminum plasma in air, Opt. Laser Technol. 122 (2020) 105862.
[11] Á. Fernández-Bravo, T. Delgado, P. Lucena, J.J. Laserna, Vibrational emission analysis of the CN molecules in laser-induced breakdown spectroscopy of organic compounds,

Spectrochim. Acta Part B At. Spectrosc. 89 (2013) 77–83.
[12] S.J. Mousavi, M. Hemati Farsani, S.M.R. Darbani, A. Mousaviazar, M. Soltanolkotabi, A. Eslami Majd, CN and C2 vibrational spectra analysis in molecular LIBS of organic materials, Appl. Phys. B 122 (2016) 106.
[13] T. Dietz, J. Klose, P. Kohns, G. Ankerhold, Quantitative determination of chlorides by molecular laser-induced breakdown spectroscopy, Spectrochim. Acta Part B At. Spectrosc. 152 (2019) 59–67.
[14] S.S. Harilal, B.E. Brumfield, N.L. LaHaye, K.C. Hartig, M.C. Phillips, Optical spectroscopy of laser-produced plasmas for standoff isotopic analysis, Appl. Phys. Rev. 5 (2018) 021301.
[15] E.N. Rao, P. Mathi, S.A. Kalam, S. Sreedhar, A.K. Singh, B.N. Jagatap, S.V. Rao, Femtosecond and nanosecond LIBS studies of nitroimidazoles: correlation between molecular structure and LIBS data, J. Anal. Atom. Spectrom. 31 (2016) 737–750.
[16] Q. Wang, A. Chen, H. Qi, W. Xu, D. Zhang, Y. Wang, S. Li, Y. Jiang, M. Jin, Influence of distance between sample surface and geometrical focal point on CN emission intensity from femtosecond laser-induced PMMA plasmas, Phys. Plasmas 26 (2019) 073302.
[17] C. Song, X. Gao, Y. Shao, Pre-ablation laser parameter effects on the spectral enhancement of 1064nm/1064nm dual-pulse laser induced breakdown spectroscopy, Optik 127 (2016) 3979–3983.
[18] Z. Cao, L. Jiang, S. Wang, M. Wang, L. Liu, F. Yang, Y. Lu, Influence of electron dynamics on the enhancement of double-pulse femtosecond laser-induced breakdown spectroscopy of fused silica, Spectrochim. Acta Part B At. Spectrosc. 141 (2018) 63–69.
[19] M. Raju, R. Singh, P. Gopinath, A. Kumar, Influence of magnetic field on laser-produced barium plasmas: spectral and dynamic behaviour of neutral and ionic species, J. Appl. Phys. 116 (2014) 153301.
[20] Y. Wang, A. Chen, S. Li, L. Sui, D. Liu, D. Tian, Y. Jiang, M. Jin, Enhancement of laser-induced Fe plasma spectroscopy with dual-wavelength femtosecond double-pulse, J. Anal. Atom. Spectrom. 31 (2016) 497–505.
[21] A. Chen, S. Li, S. Li, Y. Jiang, J. Shao, T. Wang, X. Huang, M. Jin, D. Ding, Optimally enhanced optical emission in laser-induced air plasma by femtosecond double-pulse, Phys. Plasmas 20 (2013) 103110.
[22] Y. Wang, A. Chen, Q. Wang, D. Zhang, S. Li, Y. Jiang, M. Jin, Study of signal enhancement in collinear femtosecond-nanosecond double-pulse laser-induced breakdown spectroscopy, Opt. Laser Technol. 122 (2020) 105887.
[23] A.M. Chen, Y. Wang, L.Z. Sui, S.Y. Li, S.C. Li, D.L. Liu, Y.F. Jiang, M.X. Jin, Optical emission generated from silicon under dual-wavelength femtosecond double-pulse laser irradiation, Opt. Express 23 (2015) 24648–24656.
[24] A. Hussain, M. Tanveer, G. Farid, M.B. Hussain, M. Azam, W. Khan, Combined effects of magnetic field and ambient gas condition in the enhancement of laser-induced breakdown spectroscopy signal, Optik 172 (2018) 1012–1018.
[25] S. Waheed, S. Bashir, A. Dawood, S. Anjum, M. Akram, A. Hayat, S. Amin, A. Zaheer, Effect of magnetic field on laser induced breakdown spectroscopy of zirconium dioxide (ZrO2) plasma, Optik 140 (2017) 536–544.
[26] A. Hussain, X. Gao, Z. Hao, J. Lin, Combined effects of double pulses and magnetic field on emission enhancement of laser-induced breakdown spectroscopy from aluminum plasma, Optik 127 (2016) 10024–10030.
[27] D. Wu, L. Sun, P. Liu, R. Hai, H. Ding, Enhancement of laser-induced breakdown spectroscopic signals in a liquid jet with glow discharge, Appl. Spectrosc. 72 (2018) 225–233.
[28] W. Zhou, X. Su, H. Qian, K. Li, X. Li, Y. Yu, Z. Ren, Discharge character and optical emission in a laser ablation nanosecond discharge enhanced silicon plasma, J. Anal. Atom. Spectrom. 28 (2013) 702–710.
[29] Q. Wang, A. Chen, W. Xu, D. Zhang, Y. Wang, S. Li, Y. Jiang, M. Jin, Time-resolved spectroscopy of femtosecond laser-induced Cu plasma with spark discharge, Plasma Sci. Technol. 21 (2019) 065504.
[30] Q. Wang, A. Chen, H. Qi, S. Li, Y. Jiang, M. Jin, Femtosecond laser-induced breakdown spectroscopy of a preheated Cu target, Opt. Laser Technol. 121 (2020) 105773.
[31] D. Zhang, A. Chen, Q. Wang, Y. Wang, S. Li, Y. Jiang, M. Jin, Effect of lens focusing distance on laser-induced silicon plasmas at different sample temperatures, Plasma Sci. Technol. 21 (2019) 034009.
[32] X. Yang, S. Li, Y. Jiang, A. Chen, M. Jin, Influence of distance between focusing lens and sample surface on laser-induced breakdown spectroscopy of brass at different sample temperatures, Acta Phys. Sin. 68 (2019) 065201.
[33] W. Xu, A. Chen, Q. Wang, D. Zhang, S. Li, Y. Jiang, X. Gao, M. Jin, Characteristics of laser-induced aluminum plasma plumes after increasing sample temperature and spatial confinement, J. Anal. Atom. Spectrom. 34 (2019) 2288–2294.
[34] M.S. Dawood, J. Margot, Effect of ambient gas pressure and nature on the temporal evolution of aluminum laser-induced plasmas, AIP Adv. 4 (2014) 037111.
[35] E. Vors, C. Gallou, L. Salmon, Laser-induced breakdown spectroscopy of carbon in helium and nitrogen at high pressure, Spectrochim. Acta B At. Spectrosc. 63 (2008) 1198–1204.
[36] E. Tognoni, G. Cristoforetti, Basic mechanisms of signal enhancement in ns double-pulse laser-induced breakdown spectroscopy in a gas environment, J. Anal. Atom. Spectrom. 29 (2014) 1318–1338.
[37] S. Lui, N. Cheung, Resonance-enhanced laser-induced plasma spectroscopy: ambient gas effects, Spectrochim. Acta Part B At. Spectrosc. 58 (2003) 1613–1623.
[38] M. Dong, X. Mao, J.J. Gonzalez, J. Lu, R.E. Russo, Time-resolved LIBS of atomic and molecular carbon from coal in air, argon and helium, J. Anal. Atom. Spectrom. 27 (2012) 2066–2075.
[39] X. Wang, A. Chen, Y. Wang, D. Zhang, L. Sui, D. Ke, S. Li, Y. Jiang, M. Jin, Spatial confinement effect on femtosecond laser-induced Cu plasma spectroscopy, Phys. Plasmas 24 (2017) 103305.
[40] Q. Wang, A. Chen, D. Zhang, Y. Wang, L. Sui, S. Li, Y. Jiang, M. Jin, The role of cavity shape on spatially confined laser-induced breakdown spectroscopy, Phys. Plasmas 25 (2018) 073301.
[41] J. Jia, H. Fu, H. Wang, Z. Ni, F. Dong, Effect of distance between the laser spot and the cavity center on spatially confined laser-induced copper plasma, AIP Adv. 9 (2019) 025001.
[42] X.K. Shen, J. Sun, H. Ling, Y.F. Lu, Spatial confinement effects in laser-induced breakdown spectroscopy, Appl. Phys. Lett. 91 (2007) 081501.
[43] X.W. Li, Z. Wang, X.L. Mao, R.E. Russo, Spatially and temporally resolved spectral emission of laser-induced plasmas confined by cylindrical cavities, J. Anal. Atom. Spectrom. 29 (2014) 2127–2135.
[44] Y. Wang, A. Chen, L. Sui, S. Li, D. Liu, X. Wang, Y. Jiang, X. Huang, M. Jin, Persistence of atomic spectral line on laser-induced Cu plasma with spatial confinement, Phys. Plasmas 23 (2016) 113105.
[45] N.L. LaHaye, S.S. Harilal, P.K. Diwakar, A. Hassanein, Persistence of uranium emission in laser-produced plasmas, J. Appl. Phys. 115 (2014) 163301.
[46] Y. Wang, A. Chen, L. Sui, S. Li, X. Wang, Y. Jiang, X. Huang, M. Jin, Two sequential enhancements of laser-induced Cu plasma with cylindrical cavity confinement, J. Anal. Atom. Spectrom. 31 (2016) 1974–1977.
[47] A.E. Hussein, P.K. Diwakar, S.S. Harilal, A. Hassanein, The role of laser wavelength on plasma generation and expansion of ablation plumes in air, J. Appl. Phys. 113 (2013) 143305.
[48] S.S. Harilal, T. Sizyuk, V. Sizyuk, A. Hassanein, Efficient laser-produced plasma extreme ultraviolet sources using grooved Sn targets, Appl. Phys. Lett. 96 (2010) 111503.
[49] X. Su, W. Zhou, H. Qian, Optimization of cavity size for spatial confined laser-induced breakdown spectroscopy, Opt. Express 22 (2014) 28437–28442.
[50] Y. Ueno, G. Soumagne, A. Sumitani, A. Endo, T. Higashiguchi, Enhancement of extreme ultraviolet emission from a CO2 laser-produced Sn plasma using a cavity target, Appl. Phys. Lett. 91 (2007) 231501.
[51] J. Guo, J. Shao, T. Wang, C. Zheng, A. Chen, M. Jin, Optimization of distances between the target surface and focal point on spatially confined laser-induced breakdown spectroscopy with a cylindrical cavity, J. Anal. Atom. Spectrom. 32 (2017) 367–372.
[52] C.G. Parigger, A.C. Woods, D.M. Surmick, G. Gautam, M.J. Witte, J.O. Hornkohl, Computation of diatomic molecular spectra for selected transitions of aluminum monoxide, cyanide, diatomic carbon, and titanium monoxide, Spectrochim. Acta Part B At. Spectrosc. 107 (2015) 132–138.
[53] S. Trautner, J. Jasik, C.G. Parigger, J.D. Pedarnig, W. Spendelhofer, J. Lackner, P. Veis, J. Heitz, Laser-induced optical breakdown spectroscopy of polymer materials based on evaluation of molecular emission bands, Spectrochim. Acta A Mol. Biomol. Spectrosc. 174 (2017) 331–338.
[54] H. Sun, J. Lee, H. Do, S. Im, M. Soo Bak, Experimental and numerical studies on carbon dioxide decomposition in atmospheric electrodeless microwave plasmas, J. Appl. Phys. 122 (2017) 033303.
[55] J. Wang, P. Zheng, H. Liu, L. Fang, Spectral characteristics of laser-induced graphite plasma in ambient air, Plasma Sci. Technol. 18 (2016) 1123–1129.